1997. 1(总 No. 7)

# 国际科技合作课题论文集

# SELECTED PAPERS IN SCIENTIFIC AND TECHNICAL INTERNATIONAL COOPERATION PROGRAM

中国航空研究院
CHINESE AERONAUTICAL ESTABLISHMENT

# 国际科技合作课题论文集

SELECTED PAPERS IN SCIENTIFIC AND TECHNICAL INTERNATIONAL COOPERATION PROGRAM

(7)

中国航空研究院

CHINESE AERONAUTICAL ESTABLISHMENT

航空工业出版社

AVIATION INDUSTRY PRESS

1997

《国际科技合作课题论文集》编辑部
**Editorial Department of Selected Papers in Scientific and Technical International Cooperation Program**

| | | |
|---|---|---|
| 主　编 | 崔志华 | |
| *Editor – in – Chief* | *Cui Zhihua* | |
| 编　辑 | 陈亚莉 | 冯因英 |
| *Editor* | *Chen Yali* | *Feng Yinying* |

| | | | |
|---|---|---|---|
| **通信地址：** | 北京 761 信箱 | **Address:** | P.O.Box. 761, Beijing, China |
| **邮政编码：** | 100012 | **Post Code:** | 100012 |
| **电　　话：** | 64232696 | **Tel.:** | 64232696 |
| **电　　传：** | 210467CAECN | **Tlx.:** | 210467CAECN |
| **传　　真：** | 64232507 | **Fax.:** | 64232507 |
| **出　　版：** | 航空工业出版社 | Published by China Aviation Industry Press(AIP) | |

**图书在版编目(CIP)数据**

国际科技合作课题论文集　(7)/崔志华等编. – 北京：航空工业出版社，1997.12
ISBN 7 – 80134 – 292 – 5

Ⅰ.国…　Ⅱ.崔…　Ⅲ.国防工业 – 科学技术合作 – 科研项目 – 中国 – 文集　Ⅳ.N12 – 53

中国版本图书馆 CIP 数据核字(97)第 26099 号

**航空工业出版社出版发行**
（北京市安定门外小关东里 14 号　100029）
航空工业出版社印刷厂印刷
1997 年 12 月第 1 版　　1997 年 12 月第 1 次印刷
开　本：850 × 1168　1/16　　印　张：11.75　字　数：356 千字
印　数：1 – 1000　　定　价：60.00 元

# 目　录
# CONTENTS

# 全位势方程三维机翼非定常气动力计算

CAE 南航分院　陆志良
DLR　R.Voss

**摘　要**

采用时间精确隐式近似因式分解差分格式、牛顿内迭代算法求解非定常全位势方程。边界条件及非定常尾迹条件均使用隐式嵌入处理技术以提高计算效率。解准二维附面层积分方程得到附面层位移厚度，采用粘位迭代的方法计及粘性影响。NLR7301 翼型及 LANN 机翼的计算结果说明了本文方法的有效性。

## 一、引　　言

颤振计算极大地依赖于非定常气动力的计算精度。但线性理论不能预示跨音速颤振边界出现的“凹坑”现象，必须用非线性理论来研究跨音速非定常气动力。

基于跨音速小扰动位势方程的有限差分解法最早受人们重视，目前已较为成熟。用欧拉方程甚至 N—S 方程来计算跨音速非定常气动力的研究工作也正开展之中。全位势方程方法由于精度和适用范围比小扰动方法前进一步，计算机时又比欧拉方程方法小一个数量级，在工程实践中仍有实用价值。

本文采用 C—H 型有限差分网格[1]，用时间精确隐式近似因式分解差分格式[2,3]、牛顿内迭代算法求解非定常全位势方程。边界条件及非定常尾迹条件均使用隐式嵌入处理技术以提高计算效率。鉴于粘性对激波位置有较大影响，解准二维附面层积分方程得到附面层位移厚度，采用粘位迭代的方法计及粘性影响。NLR7301 翼型及 LANN 机翼的计算结果和实验结果相吻合。

## 二、方法描述

### 1. 控制方程及分裂算法

贴体坐标下非定常全位势守恒型方程可写为

$$(\rho J)_\tau + (\rho UJ)_\xi + (\rho VJ)_\eta + (\rho WJ)_\zeta = 0 \tag{1}$$

式中 $\rho$ 为密度，$U$、$V$ 和 $W$ 是逆变速度分量，$\tau$ 为时间，$J$ 为变换 Jacobian。

方程(1)可表示成

$$F(\phi) = 0$$

其中 $\phi$ 为当前时间层上待求速度位值。用牛顿迭代法解之

$$F(\phi_*) + \left(\frac{\partial F}{\partial \phi}\right)_{\phi=\phi_*} (\phi - \phi_*) = 0 \tag{2}$$

式中 $\phi_*$ 为当前时间层上的已知值或假设值。迭代收敛时 $\Delta\phi = \phi - \phi_*$ 将趋于零。采用近似因式分解，从方程(2)可导出关于 $\Delta\phi$ 的线性方程

$$L_\xi L_\eta L_\zeta \Delta\phi = R(\phi_*) \tag{3}$$

其中

$$L_\xi = 1 + \Delta\tau U\partial_\xi - \frac{1}{\beta}\partial_\xi\rho^u Ja_{11}\partial_\xi$$

$$L_\eta = 1 + \Delta\tau V\partial_\eta - \frac{1}{\beta}\partial_\eta\rho^u Ja_{22}\partial_\eta$$

$$L_\zeta = 1 + \Delta\tau W\partial_\zeta - \frac{1}{\beta}\partial_\zeta\rho^u Ja_{33}\partial_\zeta$$

而 $\rho^u$ 为产生人工粘性的逆风密度[2]，$R$ 为方程残值。

(3) 式分三步求解

$$a.\ L_\xi\Delta\phi'' = R \quad b.\ L_\eta\Delta\phi' = \Delta\phi'' \quad c.\ L_\zeta\Delta\phi = \Delta\phi' \tag{4}$$

每步均为一三对角方程组。求解一遍后所得 $\phi$ 新值为

$$\phi = \phi_* + \Delta\phi$$

**2. 边界条件**

采用代数方法生成 C—H 型贴体网格后，$\xi$ 方向选为翼剖面表面曲线方向，$\eta$ 为展向方向，$\zeta$ 为由内向外的径向。这样，尽管方程(4a)、(4b)的未知量物理意义无明确含义，但所涉及的边界条件仅为远场边界条件和对称边界条件，不难加以实现。$\zeta$ 方向的方程(4c)可分为两部分求解，即应用物面边界条件的物面区及应用尾迹条件的自由尾迹区。

翼面上的法向速度为零，即 $W=0$。令 $i$、$j$、$k$ 分别代表 $\xi$、$\eta$、$\zeta$ 方向点序号，$k=K$ 为物面点。由 $W=0$ 可近似推得

$$\frac{\partial}{\partial\zeta}(\rho WJ)_{i,j,K} = 2(\rho WJ)_{i,j,K+\frac{1}{2}}$$

据此可得隐式物面边界条件。

因而在物面上

$$L_\zeta = 1 - \frac{2}{\beta}(\rho^u Ja_{33}\partial_\zeta)_{i,j,K+\frac{1}{2}}$$

过尾迹线压强连续，全位势下即为密度连续。得如下非定常环量传输方程

$$\Gamma_\tau + U\Gamma_\xi + V\Gamma_\eta = 0 \tag{5}$$

其中 $U$、$V$ 为尾迹上、下逆变速度平均值。通常展向分量可以忽略，方程(5)可以导出

$$\Delta\Gamma_{i,j} = \frac{\Gamma^n_{i,j} - \Gamma_{i,j} + \Delta\tau U_{i,j}(\Gamma_{i-1,j} + \Delta\Gamma_{i-1,j} - \Gamma_{i,j})}{1 + \Delta\tau U_{i,j}}$$

其中 $\Gamma^n$ 为前一时间层的 $\Gamma$ 值，$\Gamma_{i,j}$为牛顿迭代中当前时间层的已知值，$\Delta\Gamma_{i,j}$为这一已知值基础上的变化量。翼剖面后缘点 $T$(传输方程起始点)处的 $\Delta\Gamma$ 可定为

$$\Delta\Gamma_T = \Delta\phi_{T.u} - \Delta\phi_{T.l}$$

其中 $u$，$l$ 分别代表上、下后缘点。在 $\Delta\Gamma$ 已知后，将处于该点的上、下经线汇总求解各点 $\Delta\phi$，这样避免了 C 型网格下尾迹条件难以实现隐式嵌入的弱点。

**3. 粘位流迭代**

粘性会对中等强度激波的位置及强弱有较大改变。因而对于位流方法，附面层修正是改进精度的必要一环。

对机翼问题，后掠、扭转、根梢比等三维效应以及非定常因素已在位流计算中加以充分考虑。采用准定常、准二维的附面层计算已能保证一定的工程精度要求。在跨音速下，层流区很小，其影响也可忽略。假设转捩出现在吸力峰处，从此处向下游采用 Drela/Giles[4]的紊流附面层积分求解方法逐点求得附面层位移厚度。

将附面层位移厚度 $\delta^*$ 近似转化为当量翼面法向速度 $w_b$

$$w_b = u\frac{\partial\delta^*}{\partial s} = \frac{\partial\phi}{\partial s}\frac{\partial\delta^*}{\partial s}$$

其中 s 为翼剖面当地弧长坐标。该法向速度可认为由一虚拟速位 $\phi$ 的梯度所产生。翼面上

$$\nabla\phi' = w_b$$

由于 $\zeta$ 方向逆变速度分量 $W$ 可表示为

$$W = \nabla\zeta\cdot\nabla\phi$$

且 $w_b$ 与 $\zeta$ 同向，物面边界条件可写成

$$W = w_b|\nabla\zeta| = w_b\sqrt{a_{33}}$$

## 三、算例结果

用本文方法研制的程序计算了 NLR7301 翼型和 LANN 机翼的跨音速流动。图 1 为 NLR7301 翼型在来流马赫数 $M=0.7$，迎角 $a=2°$，雷诺数 $Re=2\times10^6$ 下无粘及有粘定常压力分布计算结果与实验值的比较。计算网格分别为 $135\times22$ 及 $225\times33$。两种网格下结果十分一致，粘性迭代结果与实验值 符合很好。图中可见粘流、位流的激波位置相差很大，可见计及附面层影响的必要性。

以上述状态为基础，翼型绕 40% 弦长点作俯仰谐振荡。幅值为 $\alpha_1=0.5°$，减缩频率为 $k=0.384$。图 2 显示了翼面非定常压力分布与实验值的比较。结果令人满意。

LANN 机翼的计算网格为 $161\times41\times33$，马赫数量 0.82，定常迎角 0.6°，雷诺数 $7.3\times10^6$。非定常运动以通过根剖面 62% 弦长点的平行于 y 方向的线为转动中心作俯仰运动，幅值为 0.25°，减缩频率为0.206。图 3 是定常压力分布计算结果与实验值[5]的比较。图 4 是上表面非定常压力分布实部部分与实验值的比较。图 5 是虚部比较。所有结果都符合很好。

## 四、结束语

本文给出了用全位势粘位迭代计算翼型及三维机翼跨音速非定常气动力的方法。二维定常结果显示了方法的稳定性及粘性修正的必要性。LANN 机翼的定常、非定常粘位迭代计算得到了与实验相吻合的结果。本文方法为常规跨音速气动弹性分析提供了实用、有效的工具。

## 参 考 文 献
## REFERENCES


[1] Carstens, V. Two - Dimensional Elliptic Grid Generation for Airfoils and Cascaded. DFVLR - FB 88 - 52, 1988.

[2] Shankar, V. ; Ide, H. et. al. A Fast Time - Accurate Unsteady Full Potential Schame. AIAA J. 1987, 25(2), 230 - 238

[3] Voss, R. ; Carstens, V. Computation of Unsteady Transonic Flows around Oscillating Airfoils Using FP and Euler Equations. Porc. Of the European Forum on Aeroelasticity and Structural Dynamics, DGLR, 1989, Report 89 - 1, 51 - 64

[4] Drela, M. ; Gile, M. B. Viscous - inviscid Analysis of Transonic and Low Reynolds Number Airfoils. AIAA J. 1987, 25, 1347 - 1355

[5] Zwaan, R. J. LANN Wing, Pitching Oscillation, Compendium of Unsteady Aerodynamic Measurements. AGARD Report No. 702, Addendum No. 1, 1985

# 附　图
# FIGURES

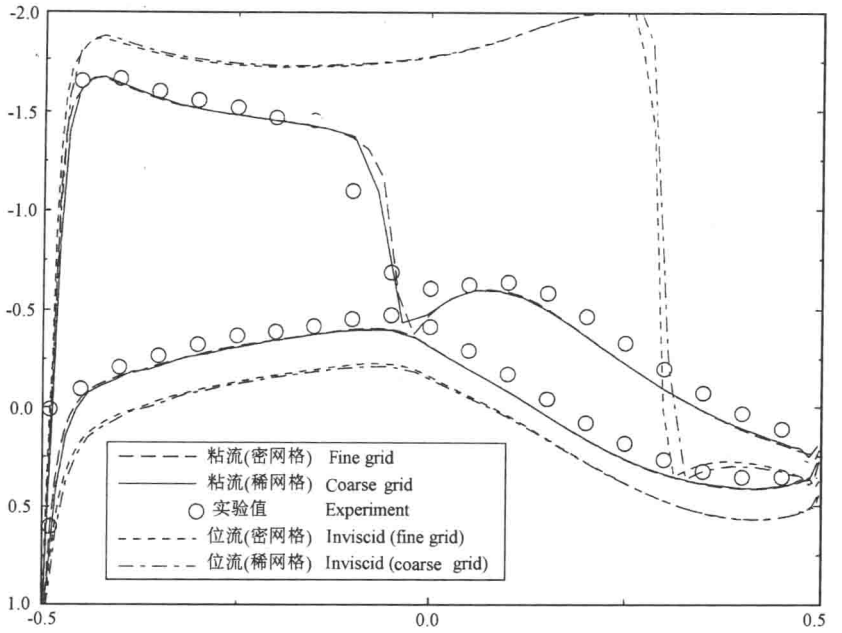


图 1　NLR7301 翼型定常压力分布，$M=0.7$，$\mathrm{Re}=2\times10^6$，$\alpha=2°$

Fig.1　Steady pressure coefficient for NLR7301 airfoil，$M=0.7$，$\mathrm{Re}=2\times10^6$，$\alpha=2°$

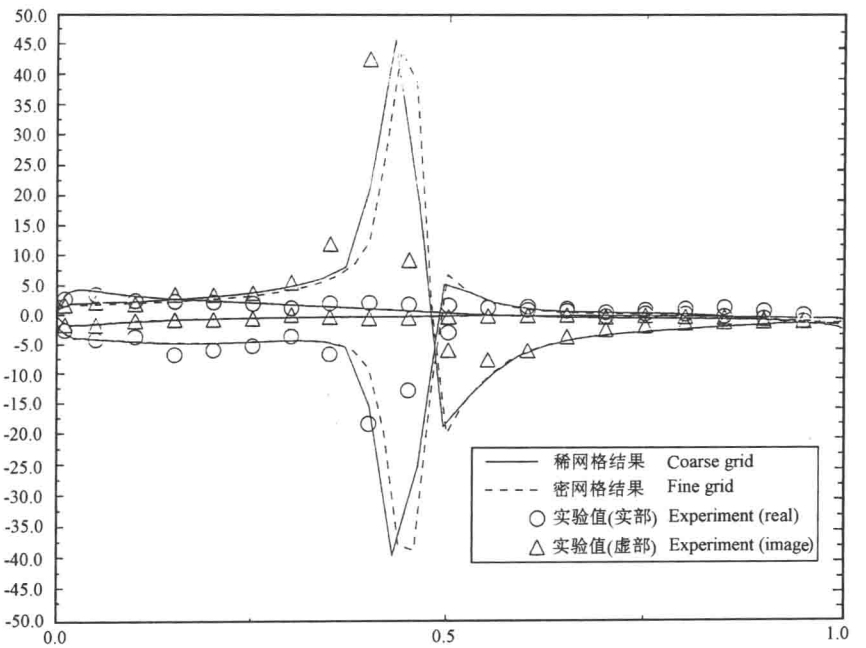


图 2　NLR7301 翼型非定常压力分布，$k=0.384$，$\alpha_1=0.5°$

Fig.2　Unsteady pressure coefficient for NLR7301 airfoil，$k=0.384$，$\alpha_1=0.5°$

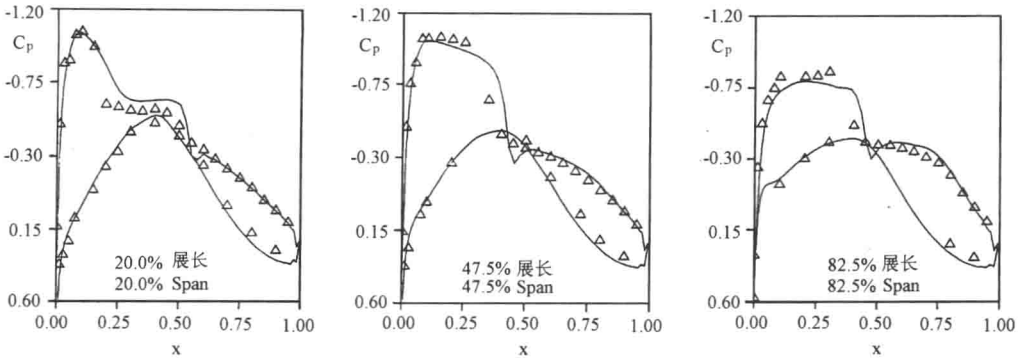


图 3　LANN 机翼定常压力分布比较，$M=0.82$，$\mathrm{Re}=7.3\times10^6$，$\alpha=0.6°$

Fig.3　Comparison of steady pressure coefficient for LANN wing, $M=0.82$, $\mathrm{Re}=7.3\times10^6$, $\alpha=0.6°$

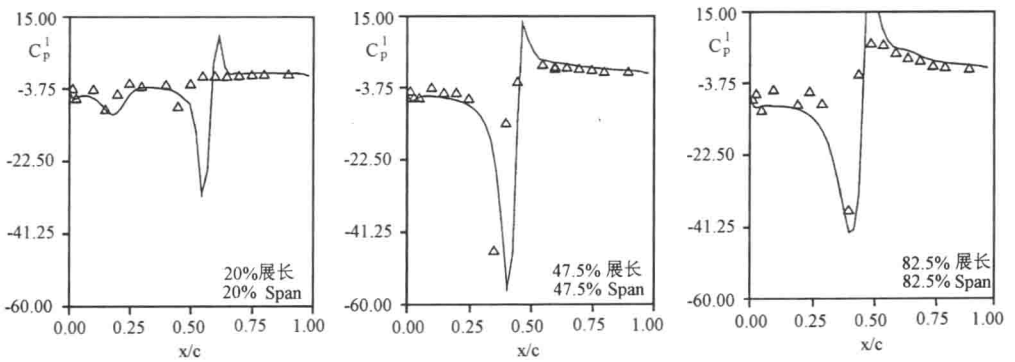


图 4　LANN 机翼上表面非定常压力分布实部比较，$k=0.206$，$\alpha_1=0.25°$

Fig.4　Upper – surface unsteady pressures comparison for LANN wing, (Real Part) $k=0.206$, $\alpha_1=0.25°$

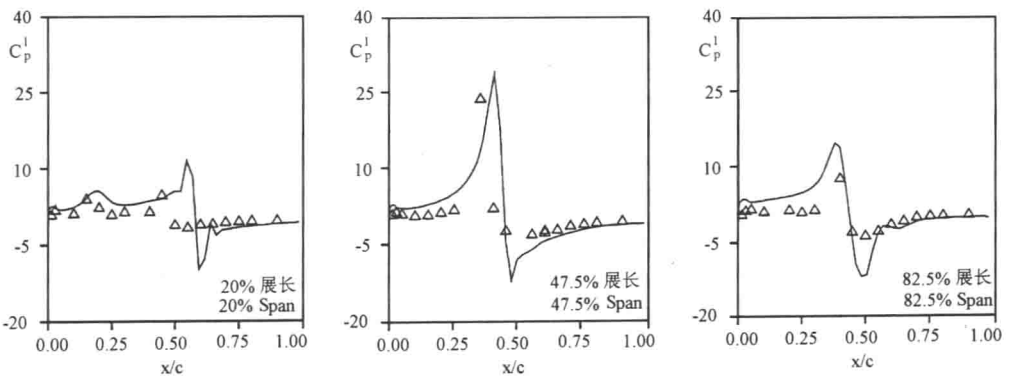


图 5　LANN 机翼上表面非定常压力分布虚部比较，$k=0.206$，$\alpha_1=0.25°$

Fig.5　Upper – surface unsteady pressures comparison for LANN wing, (Image Part) $k=0.206$, $\alpha_1=0.25°$

# COMPUTATION OF UNSTEADY TRANSONIC FLOW AROUND THE WINGUSING FULL - POTENTIAL EQUATION

Lu Zhiliang, NUAA Branch, CAE
R. Voss, DLR

**ABSTRACT**

The conservative full - potential equation and C - H grid are used to compute the unsteady transonic flows around airfoils and wings. The equation is solved by time - accurate approximate factorization algorithm and internal Newton iterations. The wake is modeled by solving the unsteady vorticity convection equation. A 2D integral boundary layer method based on the dissipation integral is used to account for viscous efforts. Calculations are presented for NLR7301 airfoil LANN wing. All results are in agreement with experimental data.

## I. INTRODUCTION

The accuracy of the flutter prediction depends mainly on the knowledge of unsteady aerodynamic forces. For unsteady transonic flows, the governing equation of flow cannot be linearized. Now methods for unsteady transonic flow calculations in order of ascending completeness of flow modeling and of computational effort are based on : Transonic Small Disturbance(TSD), Full Potential(FP), Euler equation, and Navier - Stokes equation. An important intermediate step is FP codes which need much less computation time than Euler codes and do not have restrictions of geometry as TSD. In present paper, C - H difference grid is used[1]. and a time - accurate approximate factorization algorithm is used to solve the unsteady FP equation[2,3]. At each time level, internal Newton iterations are performed to achieve time accuracy. A flux biasing technique is applied to generate proper forms of artificial viscosity. The wake is modeled by a cut behind the trailing edge across which the density is matched at any instant of time by solving the vorticity convection equation. A 2D integral boundary layer method based on the disipation integral with algebraic turbulence model of Drela/Giles is used to account for viscous efforts.

The code of this method is used to calculate the transonic flows about NLR7301 airfoil and LANN wing. All results are in agreement with experimental data.

## II. BASICS FOR THE FP ALGORITHM

### 1. Governing Equation and Approximate Factorization Scheme

The unsteady full potential equation written in a body fitted coordinate system is given by

$$(\rho J)_\tau + (\rho UJ)_\xi + (\rho VJ)_\eta + (\rho WJ)_\zeta = 0 \tag{1}$$

where $\rho$ is density. $U$, $V$ and $W$ are the contravariant velocity components in the $\xi$, $\eta$ and $\zeta$ directions. $\tau$ means

time. J is Jacobian.

Let Eq. (1) be represented as

$$F(\phi) = 0$$

where $\phi$ is the unknown to be solved at the current time plane. The Newton iteration for solution to this equation is

$$F(\phi_*) + \left(\frac{\partial F}{\partial \phi}\right)_{\phi=\phi_*} (\phi - \phi_*) = 0 \tag{2}$$

where $\phi_*$ is the currently available value of $\phi$.

At convergence, $\Delta\phi = \phi - \phi_*$, will approach zero.

Calculation of iteration matrix $\frac{\partial F}{\partial \phi}$ in Eq. (2) demands several derivative expressions, such these of $\rho$, $U$, $V$, $W$ with respect to $\phi$[2]. The method of approximate factorization is used to solve Eq. (2). In the approximate factorization procedure, the equation about $\Delta\phi$ is written as

$$L_\xi L_\eta L_\zeta \Delta\phi = R(\phi_*) \tag{3}$$

where

$$L_\xi = 1 + \Delta\tau U\partial_\xi - \frac{1}{\beta}\partial_\xi \rho^u Ja_{11}\partial_\xi$$

$$L_\eta = 1 + \Delta\tau U\partial_\eta - \frac{1}{\beta}\partial_\eta \rho^u Ja_{22}\partial_\eta$$

$$L_\zeta = 1 + \Delta\tau U\partial_\zeta - \frac{1}{\beta}\partial_\zeta \rho^u Ja_{11}\partial_\zeta$$

and $\rho^u$ denotes the upwind density to produce the necessary artificial viscosity.

Eq. (3) is solved in three steps

$$a.\ L_\xi \Delta\phi'' = R \qquad b.\ L_\eta \Delta\phi' = \Delta\phi'' \qquad c.\ L_\zeta \Delta\phi = \Delta\phi' \tag{4}$$

Each one results in a tridiagonal matrix equation, and the new f is given by

$$\phi = \phi_* + \Delta\phi$$

## 2. Boundary Conditions

The grid generation is obtained by a method presented in Ref. (1). C - H grid is used. Although the variables in Eq. (4a) and Eq. (4b) are two complicated functions with little physical meaning, it is not difficult to impose the far field and symmetry plane boundary conditions to Eq. (4a) and (4b). The original variable $\Delta\phi$ in Eq. (4c) makes it possible to apply flow tangency condition on the body surface and unsteady wake condition on the cut line exactly.

On the wing surface, the contravariant velocity component $W$ has to vanish : $W = 0$. Let i be the running index in the $\xi$ direction, j in the $\eta$ direction, k in the $\zeta$ direction, and $k = K$ denotes the body point. From $W = 0$ the follow relationship is given

$$\frac{\partial}{\partial\zeta}(\rho WJ)_{i,j,k} = 2(\rho WJ)_{i,j,k+\frac{1}{2}}$$

Eq. (4c) for the body points can be represented as

$$L_\zeta = 1 - \frac{2}{\beta}(\rho^u Ja_{33}\partial_\zeta)_{i,j,k+\frac{1}{2}}$$

The pressure is continuous across the cut line. In the full potential framework, this results in the continuity of density. An unsteady transport equation for the potential jump across the wake can be written as

$$\Gamma_\tau + U\Gamma_\xi + V\Gamma_\eta = 0 \tag{5}$$

where $U$ and $V$ are the averages of contravariant velocities above and below the wake. In general case the compo-

nent in $\eta$ direction can be neglected and the Eq. (5) can be treated as

$$\Delta\Gamma_{i,j} = \frac{\Gamma^n_{i,j} - \Gamma_{i,j} + \Delta\tau U_{i,j}(\Gamma_{i-1,j} + \Delta\Gamma_{i-1,j} - \Gamma_{i,j})}{1 + \Delta\tau U_{i,j}}$$

where $\Gamma^n$ is the currently available value. The vorticity value at the trailing edge (point $T$) is given by

$$\Delta\Gamma_T = \Delta\phi_{T.u} - \Delta\phi_{T.l}$$

where the subscripts u, l stand for up surface and lower surface.

### 3. Viscous Inviscid Interaction

The effect of viscosity can cause the inviscid simulation of moderately strong shock case to be inaccurate. Boundary layer correction is a necessary step to improve the inviscid results.

The three – dimensionality of the wing, due to sweep, taper and twist, was considered by the inviscid solution which provided the boundary condition at freestream for the boundary layer solution. A two dimensional boundary layer is calculated at each cross section of the wing span at each time step or after several steps. In transonic flow, the laminar region is very small, the effect on the aerodynamic performances is insignificant. The dissipation integral with algebraic turbulence model is used. This yields the boundary layer thickness distribution, which is used to modify the surface tangency boundary condition.

Along the wing surface, the corresponding blowing velocity can be given by

$$w_b = u\frac{\partial\delta^*}{\partial s} = \frac{\partial\phi}{\partial s}\frac{\partial\delta^*}{\partial s}$$

where s is the cross section surface of the wing span. It can be regarded as the gradient of a velocity potential induced by viscosity. On the body surface

$$\nabla\phi' = w_b$$

Since the contravariant velocity component in the $\zeta$ direction can be written as

$$W = \nabla\zeta \cdot \nabla\phi$$

with $w_b$ and $\zeta$ in the same direction along the wing surface, the body condition then becomes

$$W = w_b|\nabla\zeta| = w_b\sqrt{a_{33}}$$

## III. PRESENTATION OF RESULTS

The code of this method is used to calculate the transonic flows about NLR7301 airfoil and LANN wing. The 2D steady test results have been obtained on a C – type grid with 225 × 33 nodes and a coarse grid of 135 × 22 nodes, which are shown in fig. 1. The same figure shows the comparison of steady pressure distributions obtained by viscous and inviscid computations on both grids and from experiment. The influence of viscous effects is significant and shows up in a tremendous shift of shock position and shock strength. The agreement of the computations with test results is good.

Unsteady computations have been carried out again on both grids. Looking at the unsteady pressure distribution (first harmonic component) on the surface in fig. 2, the results for the different grids differ only in the region of the pressure pulse caused by the oscillating shock wave. The agreement with test results is good.

For the 3D case, we present results of computations for the LANN supercritical wing and the AGARD steady and unsteady test case CT5[5], see fig. 3 , 4 and 5. Results have been obtained on a C – H type grid with 161 × 41 × 33 nodes. The Mach number is 0.82 and the steady angle of attack is 0.6 degrees. Reynolds number is 7.3 million with root chord as reference length. The unsteady test case in fig. 4 is about rigid harmonic pitching about an axis through 62% root chord. Pitching amplitude is 0.25 degrees and reduced frequency is 0.206 with root

chord as reference length. All results are in agreement with experimental data.

## IV. CONCLUSION

A time – accurate approximate factorization algorithm is used to solve the unsteady FP equation. A 2D integral boundary layer method is used to account for viscous efforts. The steady and unsteady transonic flows about NLR7301 airfoil and LANN wing are calculated. The 2D results show the stability of this method and the influence of viscous effects. The results of 3D steady and unsteady transonic flow for LANN wing are in agreement with experimental data.

# 高升力大堵塞洞壁干扰修正

CAE　南航分院　张文华
DLR　H.Otto

**摘　要**

本文采用洞壁上最佳点所测得的壁压和算出的影响函数对三元高升力大堵塞模型进行洞壁干扰修正试验研究。修正结果表明，该方法对高升力大堵塞模型的升力、阻力和力矩的修正是可行的。

## 符　号　表

| | |
|---|---|
| $\alpha$ | 迎角 |
| $q_\infty$ | 来流动压 |
| $C_P$ | 压力系数 |
| $f_A$ | 下洗修正影响函数 |
| $f_V$ | 堵塞修正影响函数 |
| $\nu$ | 模型展长与风洞宽度比 |
| $C_y$ | 测量的升力系数 |
| $C_x$ | 测量的阻力系数 |
| $C_m$ | 测量的俯仰力矩系数 |
| $k$ | 修正系数 |
| $l$ | 模型展长 |
| $B$ | 风洞宽度 |
| $H$ | 风洞高度 |
| | 下标 |
| $W$ | 洞壁 |
| $M$ | 模型 |
| $H$ | 平尾 |
| $K$ | 洞壁修正 |
| 1 | 前测量面 |
| 2 | 后测量面 |

## 一、引　　言

在洞壁干扰修正研究中，Glauert 提出了最古老的修正方法[1]，其方法仅适用于小迎角小堵塞情况。Schulz[2]提出的壁压修正法，用的测压点少，可用于高升力的修正，但方法只能适用于矩形风洞。Hackett[3]提出的修正方法，由于需要模型的气动特性详尽描述，因而所需测压点较多，提高了计算成本。Holst[4]提出的所谓 Green 修正法，其方法是否适用于高升力大堵塞情况有待验证。Labrujere[5]提出的 MBC 方法，对高升力模型试验研究给出了好的结果，遗憾的是对力矩的修正不尽人意。文献[6]提出的壁压影响函数法(WPIF 法)，可适用于矩形切角风洞，且用高升力中平尾模型 SWIM 进行了试验验证，在小风洞中其 $\nu=0.73$，力和力矩测量结果经修正后与大风洞中实验数据基本一致。如果平尾为高平尾，模型展长与风洞宽度之比 $\nu$ 达到 0.8，WPIF 法是否适用，本文即讨论此问题。

## 二、基本方法与公式

壁压影响函数法的关键是找出洞壁上任意一点壁压与模型所在点速度修正值之间的关系式。按文

献[2]，只存在上洗效应时有

$$\Delta\alpha_M = -(1/2f_A)\Delta C_{PW}(A) \tag{1}$$

式中 $f_A = \Delta V_{XW}(A)/\Delta V_{ZM}(A)$，只存在阻塞效应时则有

$$\Delta q/q_\infty = -(1/f_V)\Delta C_{PW}(V) \tag{2}$$

式中 $f_V = \Delta V_{XW}(V)/\Delta V_{XM}(V)$。$f_A$ 和 $f_V$ 可用修正网格法[7]求出。对于 NWB[8]（不伦瑞克低速风洞）算出的 $f_A$ 和 $f_V$，其结果见文献[9]，其具有聚焦特性。只是含有 $\nu = 0.8$ 情况下聚焦特性比没有 $\nu = 0.8$ 的略差。在横向聚焦点求出的基础上，采用两平面法算出组合影响函数 $f_{A12}$ 和 $f_{V12}$ 以及相应的修正系数、测量系统坐标。其结果列于表 1

**表 1　NWB 风洞测量系统及修正系数**

| 修正类型 | 测量系统坐标 | | | | 修正常数 | | | |
|---|---|---|---|---|---|---|---|---|
| | $\xi_{W1}$ | $\xi_{W2}$ | $\eta_W$ | $\zeta_W$ | $K_1$ | $K_2$ | $\bar{f}_{V12}$ | $\bar{f}_{A12}$ |
| 堵　塞 | −0.240 | +0.680 | ±1.0 | ±0.761 | 1.0005 | 0.9993 | 2.5438 | |
| 下　洗 | −0.325 | +0.936 | ±0.9 | ±1.00 | 0.9998 | 0.9989 | | 1.8642 |

表中 $\xi = 2x/B$，$\eta = 2y/B$，$\zeta = 2Z/H$。图 1 给出 *NWB* 风洞用于下洗和堵塞修正的测量系统。

利用两平面法，修正公式(1)(2)此时改变为

$$\Delta\alpha_M = -(1/2\bar{f}_{A12})(K_1(A)\Delta C_{PW1}(A) + K_2(A)\Delta C_{PW2}(A)) \tag{3}$$

$$\Delta q/q_\infty = -(1/\bar{f}_{V12})(K_1(V)\Delta C_{PW1}(V) + K_2(V)\Delta C_{PW2}(V)) \tag{4}$$

式中 $\bar{f}_{A12}$ 和 $\bar{f}_{V12}$ 为组合影响函数 $f_{A12}$ 和 $f_{V12}$ 的几何平均值[2]。由文献[2]可知

$$\Delta C_{PW1}(V) = 1/2(\Delta C_{P1S} + \Delta C_{P1d})$$

$$\Delta C_{PW1}(A) = 1/2(\Delta C_{P1S} - \Delta C_{P1d})$$

$\Delta C_{P1S}$，$\Delta C_{P1d}$ 分别表示前测量面对应于模型吸力面或压力面的洞壁上最佳点测出的压差系数。速压、迎角、气动系数修正公式为

$$q_k = q_\infty + \Delta q$$

$$\alpha_k = \alpha + \Delta\alpha_M$$

$$C_{yk} = (C_y + \Delta C_y)(1 + \Delta q/q_\infty)$$

$$C_{xk} = (C_x + \Delta C_x)(1 + \Delta q/q_\infty)$$

$$C_{mk} = (C_m + \Delta C_m)(1 + \Delta q/q_\infty)$$

式中 $\Delta C_y = (F_H/F_W)(l_1/H)(\partial C_y/\partial\alpha)\omega\Delta\alpha_M$，$\Delta C_x = C_y\sin\Delta\alpha_M$，$\Delta C_m = (F_H/F_W)(l_1/b_A)(l_2/H)(\partial C_y/\partial\alpha)\omega\Delta\alpha_M$，$\omega$ 是弯曲常数[2]，$F_H$ 和 $F_W$ 分别为平尾和机翼的平面面积，$l_1$ 为机翼 1/4 平均弦点至平尾 1/4 平均弦点间距离，$l_2$ 为力矩参数点至平尾 1/4 平均弦点间距离，$b_A$ 为机翼平均弦弦长。

## 三、实验模型和风洞

实验模型为 DLR(德国宇航院)和 COMO 模型(洞壁干扰修正用模型)，其为带襟翼的高升力高平尾模型。通过机翼展向两端小段的增除，其翼展可为 2.6m 或 2.4m。模型由四个不同部分组合而成：*R*(机身)、*F*(机翼)、*H*(平尾)、*K*(襟翼)。模型详情见图 2。

实验分别在 DLR 的 NWB 和 DNW(德国荷兰风洞)中进行。NWB[8]系低速闭口风洞，实验段为矩形，其实验段尺寸为 3.25m(宽)×2.8m(高)×8m(长)。模型由尾撑和弯刀支撑。模型最大展长与风洞宽度之比 $\upsilon$ 为 0.8。DNW 亦系低速风洞，所进行的实验段尺寸为 8m(宽)×6m(高)×20m(长)，此

时 $\nu = 0.325$，机翼平面面积与实验段横截面面积之此为 0.01488，近似认为模型在该风洞中进行的实验为无洞壁干扰数据。

## 四、结　　论

在 NWB 洞壁上进行了壁压测量。用有模型时的洞壁壁压数据减去无模型仅有支架时的洞壁壁压数据，得出我们所需的纯模型诱导的洞壁壁压数据，其随迎角和轴向变化情况见文献[9]。应用前述给出的修正公式可以对测量的力和力矩进行修正计算。图 3、4、5 给出了模型 COMO 在 RFKH2 构型下(即有机翼、机身、平尾、襟翼，$l = 2.6$m)测量的结果和用本文以及文献[10]的修正计算结果。从比较可以看出，结果是合理的，本文的修正计算结果与文献[10]的计算基本一致。然而本文只需 16 最佳点测压数据，而文献[10]则需要很多。可见 WPIF 法可用于高升力高平尾及大堵塞情况。

DNW 的数据在晚些时候的文献中发表，其中还将包含新近 DLR 和 NLR(荷兰宇航院)研究的对 NWB 的所获 COMO 数据修正计算结果。

## 参 考 文 献

## REFERENCES


[1] Glauert H. Wind tunnel interference on wings, bodies and aircrews. ARC R&M 1566, 1933

[2] Schulz G. Ein universelles dreidimensionales Wanddruck Korrekturverfahren für geschlossene rechteckige Unterschall windkanalmeβstrecken(Verdrängung, Abwind, Krümmung). DFVLR FB82-18, 1982

[3] Hackett J E. A Review of the"Wall Pressure Signatur" and other Tunnel Constraint Correction Methods for High Angle of Attack Test. Lockheed-Georgia Company, Maritta, Georgian, USA, 1981

[4] Holst H. Verfahren zur Bestimmung von dreidimensionalen Windkanalwandinterferenzen und Wandadaption mit Hilfe gemessener Wanddrücke bei kompressibler Unterschallströmmung. DLR FB90-46, 1990

[5] Labrujere Th E, Maarsingh R A, Smith J. Evaluation of Messured-Boundary-Condition Methods for 3D Subsonic Wall Interference. NLR TR88072 U, 1988

[6] Zhang W H, Küpper A. Windkanalmessungen zur Überprüfung eines dreidimensionalen Wanddruck-korrekturverfahrens für geschlossene Meβstrecken. DLR IB19111-92A11, 1992

[7] Holst H. German Activies on Wind Tunnel Corrections. AGARD Report 692, 1982

[8] Kausche G, Otto H, Christ D, Siebert R. Der Niedergeschwindigkeits-Windkanal der DFVLR in Braunschweig. DFVLR-Mitt, 88-25, 1988

[9] Zhang W H, Otto H. WindKanal Wandinterferenzenkorrektur für geschlossene Unterschallwindkanalmeβstrecken. DLR IB19111 - 96A11, 1996

[10] Küpper A. Kraft-und Wanddruckmessungen und Korrektur an einen subsonischen Wandinterferenzen-Modell im Niedergeschwindigkeits-Windkanal Braunschweig. DLR IB19111-94A02, 1994

# 附　图
# FIGURES

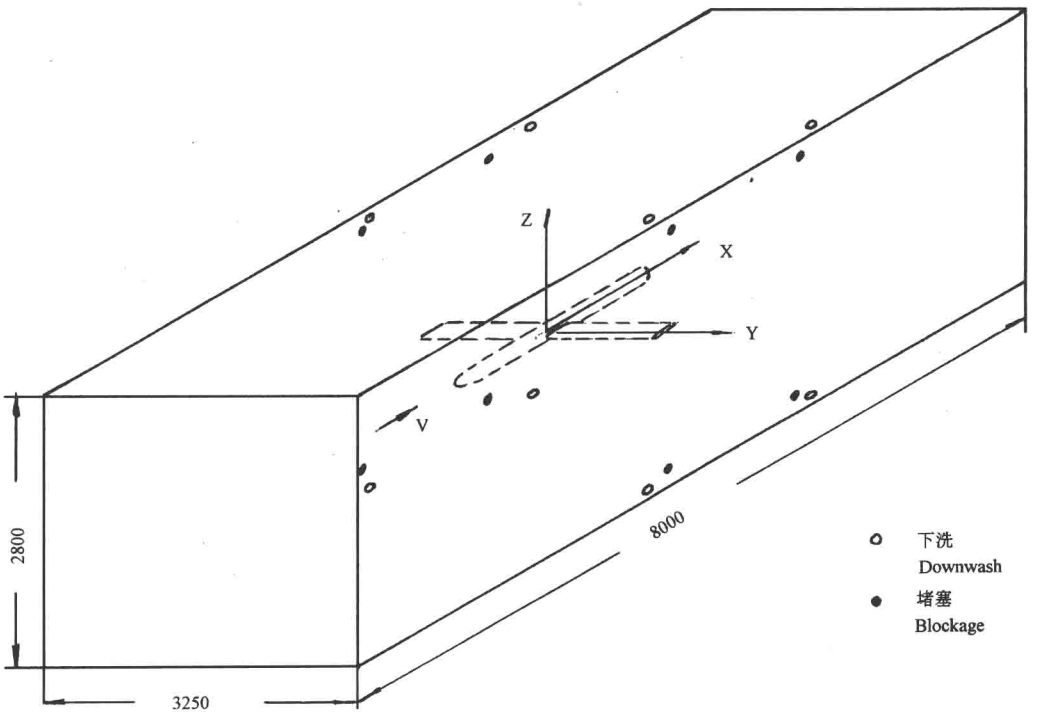


图 1　风洞壁压测量系统

Fig.1　Wall pressure measurement systems